

Control of polarization-induced stiffness asymmetry in highly focused optical tweezers

Jinmyoung So¹ and Jai-Min Choi^{1,2,*}

¹*Division of Science Education, Chonbuk National University, Jeonju 561-756, Korea*

²*Institute of Fusion Science, Chonbuk National University, Jeonju 561-756, Korea*

[*jaiminchoi@jbnu.ac.kr](mailto:jaiminchoi@jbnu.ac.kr)

Optical tweezers that utilize a highly focused, linearly polarized laser beam are shown to exhibit strong stiffness asymmetry, which originates from the anisotropic field distribution in the transverse plane. We present an experimental demonstration in which the degree of stiffness asymmetry is controlled by using the polarization state of the trapping beam as a tuning knob. Theoretical support for the experimental observations is provided based on the generalized Lorenz-Mie theory, which is revised to encompass the general polarization state of a trapping beam.

OCIS codes: (140.7010) Laser trapping; (350.4855) Optical tweezers or optical manipulation.

1. Introduction

A tightly focused laser beam can allow radiation pressure to be overcome, resulting in the stable optical trapping of microscopic particles in an optical potential; this principle is physically realized in instruments known as “optical tweezers” (OT) [1, 2]. Contactless optical clamping methods provide an promising research platform that could be effectively decoupled from a thermal reservoir (e.g., achieving the ground state cooling in cavity optomechanics [3]); they also offer additional means of governing the system dynamics (e.g., studying interaction dynamics in colloidal systems [4, 5] and microgyroscope applications [6, 7]). Moreover, by harnessing the extreme force sensitivity involved

(i.e., as low as 100 aN [8]), such methods find versatile applications in biophysics and precision control [9]. In these applications, tailoring the landscape of the optical potential is of significant import, and considerable effort has also been devoted to engineering the optical potential in order to realize the modeled systems desirable for manifesting novel characteristics of research interest. Recent researches on this subject in the context of highly focused OT show that a strong asymmetry in trap stiffnesses, which is equivalent to asymmetric trap potential, is due to the anisotropic electromagnetic (EM) field distribution in the transverse plane of the laser beam's path [10-12]. The focused EM field distribution formed by an objective lens having a high numerical aperture (NA) is well described by the angular spectrum method based on vectorial diffraction theory [13-15] and the resulting optical potential is rendered via light-matter interaction. Rohrbach *et al.* illustrated the trap stiffness asymmetry, both theoretically and experimentally, in their OT setup based on a water-immersion objective lens [10]. Additionally, Zakharian *et al.* used the finite-difference time-domain (FDTD) method to investigate polarization effects on the optical potential formed in air and in water [11]. Furthermore, the recent research of Madadi *et al.* explores the aberration effect that is caused by the refractive index mismatch between the interfaces of the media involved; more specifically, they investigated the trap potential asymmetry that arises in OT composed of an oil-immersion objective lens [12]. In this paper, we address the asymmetry of trap stiffness in highly focused OT and demonstrate control over the stiffness asymmetry using the polarization state of the trapping beam.

To investigate the effect of the polarization state of the trapping beam on the trap potential asymmetry, we constructed a custom-built OT setup equipped with polarization control. The input beam is prepared with a linear, elliptic, and circular polarization, and the resulting trap potential asymmetry is characterized in terms of the trap stiffnesses (i.e., spring constants) in the transverse plane. The trap stiffnesses are measured for each polarization state from the motion of trapped particles using the back focal plane interferometry (BFPI) technique [8]. As was demonstrated in the referred works [10-12], the landscape of the optical potential depends not only on the EM field distribution in

the trapping region, but also on the characteristics of the particle being trapped, i.e., its size, shape, and index of refraction and the index of refraction of the solvent medium. In this study, we focus on the systematic investigation of the polarization effect on the trap potential asymmetry using the polystyrene spheres with diameter of 300 ± 15 nm.

2. Experimental apparatus and preliminary measurement

We constructed a custom-built OT setup equipped with polarization control, as shown in Fig. 1(a). The output of the diode laser system is fed to the tapered amplifier, resulting in 1.6 W of output power with a tuned wavelength of 780 nm. The power-amplified beam is guided to the experimental region through a single-mode polarization-maintaining fiber. The first half-wave plate (HWP1) and polarizing beam splitter (PBS) were used to adjust the input beam power, whereas the second half-wave plate (HWP2) and the quarter-wave plate (QWP) provided tuning knobs for polarization control. As benchmark conditions, the incident beam power and the collimated beam size before the water-immersion objective lens (UPLSAPO 60XW, Olympus) were set to 250 mW and 4 mm (corresponding to a filling factor of ~ 1), respectively. The wave plates were initially aligned to produce linearly polarized light along the horizontal direction in the laboratory frame: $\vec{E}_{in} = E_0 \hat{x}$. A 170 μm thick cover glass (NO1.5H, ZEISS) and a nominal slide glass were sandwiched together as sidewalls in order to construct the sample chamber using 200 μm thick, double-sided 3M tape. The 300 ± 15 nm polystyrene spheres (NT08N, Bangs Laboratories) were diluted and dispersed in deuterium oxide (D_2O) in order to minimize heat-induced convection. Additional procedures for the hydrophobic coating of glass surfaces and stabilizing surfactant were made following the protocol provided in Ref. [16]. The aspheric condenser lens (L1) collects part of the trapping beam together with the scattered light. The superposed field pattern in the back focal plane of L1 was imaged onto the quadrant photodiode (QPD) via the relay lens L2, which is known as the BFPI technique [8]. An iris at the back focal plane of L1 was used to optimize the sensitivity of BFPI by adjusting the effective NA of the condenser lens [17] and the

auxiliary components (LED, L3, and DM) that are part of the imaging setup. Having a diffraction-limited spot is crucial for our research because it ensures exclusion of other contributions, e.g., aberration effects, to the potential landscape and trap asymmetry itself strongly depends on the spot size. In the experimental setup, we exploited the scattered light from the particle to produce a spot that is as tight as possible. For a circularly polarized trapping beam, part of the scattered light, which was recollectd by the objective lens, passed the QWP again, mostly resulting in a polarization that was rotated by 90° (\hat{y}). The rotated scattered light was redirected by the PBS and mode-filtered using a $15\ \mu\text{m}$ pinhole to eliminate the reflected light from the other interfaces, except for that of the trapped particle. We maximized the guided power by adjusting the beam alignment and the correction collar of the objective lens [18].

The output signals ($\delta V_x, \delta V_y, V_{SUM}$) of QPD were logged using a high-speed digital scope (5444B, PicoScope) with a $5\ \mu\text{s}$ sampling time; each measurement was performed over the course of 2 s. The beam power in the medium was estimated to be 40 mW. Part of the δV_x (red points) and δV_y (blue points) data are presented in Fig. 1(b), and the corresponding power spectral density (PSD) is shown in Fig. 1(c). The stochastic motion of the trapped particle can be modeled in the form of the Langevin equation with an additional Hookean force term, where the restoring force in a specific direction is characterized by the corresponding stiffness (i.e., the spring constant) k_i , where $i \in (x, y, z)$. The power spectra for each degree of freedom can be approximated to Lorentzian function $S_i(f) = (D/2\pi^2)/(f_{c,i}^2 + f^2)$ [19], where D is the diffusion constant, the corner frequency $f_{c,i}$ is given by $k_i/2\pi\gamma$, and γ is the frictional constant given by Stokes' law, $\gamma = 6\pi\eta a$; we used a dynamic viscosity of $\eta_{D_2O} = 1.12 \times 10^{-3}\ \text{kg/s}\cdot\text{m}$ and a radius of $a = 150\ \text{nm}$. The thick solid lines (red and blue curves in Fig. 3(c)) are the results of the Lorentzian fit following the procedures outlined in Ref. [20], which give corner frequencies of $(f_{c,x}, f_{c,y}) = (2497, 3616)\ \text{Hz}$, respectively. The associated trap stiffnesses for each

degree of freedom are $(k_x, k_y) = (49, 71)$ pN/ μm , which yields a trap asymmetry factor of $s_{A, \hat{x}} = 0.31$ for the linearly (\hat{x}) polarized trap beam.

3. Characterization and control of stiffness asymmetry

3.1 Mathematical underpinnings

We revised the previously developed GLMT-based force calculation to include the general input polarization state for our study. We briefly state procedures for the GLMT calculation using a high-order Gaussian beam developed by Barton *et al.* [21, 22]. (Detailed expressions can be found therein.) The optical force exerted on a spherical particle is given by the surface integral of the Maxwell stress tensor over the enclosed surface of the particle [22]. The associated EM fields in the Maxwell stress tensor consist of the incident field and the scattered field in the surrounding medium. The EM fields can be represented by a series expansion of Riccati-Bessel functions and spherical harmonics $Y_{lm}(\theta, \phi)$ with the following expansion coefficients: (A_{lm}, B_{lm}) for the incident field and (a_{lm}, b_{lm}) for the scattered field, where l and m are mode numbers. The coefficients a_{lm} and b_{lm} are given by Mie coefficients and the coefficients of the incident field A_{lm} and B_{lm} . The fifth-order Gaussian beam method provides the approximated functional form of the tightly focused EM fields, and the coefficients A_{lm} and B_{lm} can be extracted via the numerical integration of the EM field function multiplied with $Y_{lm}^*(\theta, \phi)$, where “*” denotes complex conjugation. To include the general polarization states, the EM field components are transformed using the standard Jones matrices of rotation and phase retardation. Finally, the optical force is evaluated using the reorganized expressions (see Eqs. (5) and (6) in Ref. [22]), with the properly chosen truncation mode number $l = l_{\text{max}}$; the integral representation of the optical force is simplified in a series that includes the coefficients a_{lm} , b_{lm} , A_{lm} , and B_{lm} .

Although the fifth-order Gaussian beam could represent the tightly focused EM field distribution with an error of a few percent for the parameter $s \sim 0.3$ ($=1/2pw_0$), the minimum beam spot size needs to

be obtained from another method that can encompass experimental parameters such as the NA of the objective lens, the filling factor, the apodization effect, and the refractive index mismatched aberration effect [14, 15]. The angular spectrum method, which is based on vectorial diffraction theory, estimates the minimum spot size to be 293 nm for the following experimental parameters: NA = 1.2, filling factor = 1.0, wavelength $\lambda = 780$ nm, and the index of refraction of deuterium oxide (D₂O) $n_m = 1.324$. In comparison with our experimental results, the beam waist (w_0) is chosen to be 300 nm, which is 2% larger than the ideal case, although we elaborated to produce the tightest spot size as possible. It may be worth noting that the spot size is estimated through a Gaussian fit of the numerically calculated field pattern [17], whereas conventional definition of optical resolution (radius of the primary Airy disk) gives the relevant value 270 nm.

We present numerical calculation results for two extreme cases of linear and circular polarization. The normalized electric field strength at the focal plane is shown in Fig. 2(a) for a linearly (\hat{x}) polarized input beam. The dashed white line outlines the e^{-1} level of the field strength, and clearly shows an elongated distribution along the \hat{x} direction. The upper panel of Fig. 2(b) shows the intensity profiles along the lines L_x and L_y, and the lower panel shows the relative difference of the calculated intensity profiles between the fifth-order Gaussian beam method and the method based on vectorial diffraction theory; it can be seen that the maximum fractional difference between the two methods is less than 2%. The GLMT calculation results of optical the force components, F_x and F_y, on a 300 nm polystyrene particle are presented in Fig. 2(c). The restoring force along the elongated direction (\hat{x}) is small compared to that of the other direction (\hat{y}) for a given displacement (e.g., $-w_0/2 \sim w_0/2$). The resulting stiffness asymmetry, $s_A = 1 - k_x/k_y$, is 0.28. The trap stiffnesses, k_x and k_y , were calculated by performing a polynomial fit of the numerically calculated optical force around the origin. We note that the stable trap position along the beam propagation direction (\hat{z}) pushes away from the focal point ($z = 0$) to $z = 234$ nm owing to the scattering force. Figure 3 presents the distribution of the electric field

strength, the designated intensity profiles, and the resulting optical forces for a circularly polarized input beam with the same experimental parameters. It shows an isotropic field distribution in the focal plane, and the trap stiffness asymmetry is estimated to be zero (i.e., $s_A = 0$) within the precision of the numerical calculation.

3.2 Experimental results

Polarization-induced stiffness asymmetry was systematically investigated as a function the prepared input polarization state. The experimental parameters used in the case of the preliminary experiment in Fig. 1 are used here again. The angular variation of the trap stiffnesses $k_x(\theta)$ and $k_y(\theta)$ are estimated from the PSD measurements for a linearly polarized input beam rotated by $2\theta_{HWP}$: $\vec{E}_{in} = E_0(\hat{x}\cos 2\theta_{HWP} + \hat{y}\sin 2\theta_{HWP})$. GLMT calculations are compared with the experimental results in Fig. 4(a), where k_x and k_y are stiffnesses along the horizontal and vertical direction in the laboratory frame, respectively (referred to as the QPD segmentation axes). The average value of the experimentally measured trap stiffness, $\bar{k}_{EXP} = (\bar{k}_x(\theta) + \bar{k}_y(\theta))/2$, was 59.2 pN/ μm (the dashed horizontal line), whereas the GLMT calculation shows $\bar{k}_{GLMT} = 59.5$ pN/ μm (the solid horizontal line). From the angular measurements, the stiffness asymmetry is estimated to be $\bar{s}_{A,EXP} = 0.29$, whereas the GLMT calculation gives $\bar{s}_{A,GLMT} = 0.28$. A demonstration of trap asymmetry control, which proceeds by adjusting the polarization state of the input beam, is presented in Fig. 4(b). The polarization state of the input beam is prepared as $\vec{E} = E_0(\cos\theta_{QWP}\hat{x} + e^{i\delta}\sin\theta_{QWP}\hat{y})$, where θ_{QWP} is the angle between the slow axis of the QWP and the horizontal axis (\hat{x}) and the phase retardation $\delta = \pi/2$ for a quarter wave plate. As the polarization state becomes circular at $\theta_{QWP} = 45^\circ$, the strong asymmetry of trap stiffness diminishes, which can be inferred from the isotropic field distribution of a circularly polarized beam, as discussed in the context of Fig. 3. The balanced stiffness asymmetry via polarization control is found to be $s_A = 0.02$ for a circularly polarized beam measured at $\theta_{QWP} = 45^\circ$. Systematic deviations of $k_x(\theta)$ and $k_y(\theta)$ between the

experimental results and the theoretical calculations can be attributed to uncontrolled aberrations and beam power calibration.

To explore the trap potential landscape formed by a circularly polarized beam in the transverse plane, we investigated the angular variation of the balanced trap stiffnesses in the following way. For each angle of HWP2, the direction of the input beam polarization is rotated to $2\theta_{HWP}$, and the QWP is rotated to produce the circularly polarized input beam: $\theta_{QWP} = 2\theta_{HWP} + 45^\circ$. Figure 5(a) shows moderate variation of the stiffnesses $k_x(\theta)$ and $k_y(\theta)$ compared to the previously discussed angular variation of the trap stiffnesses for linearly polarized light in Fig. 4. The average stiffness (solid line) is 59.4 pN/ μm with the 1σ -level standard deviation (dashed lines) of 0.9 pN/ μm corresponding to fluctuations of 1.4%. Another measurements (not presented) of the change in trap stiffness as a function of the trap depth over the range of 10–150 μm show random fluctuations of only a few percent, as is typical for a water-immersion objective lens [12, 15]. Figure 5(b) shows the linear dependence of trap stiffnesses on the beam power for the cases of linear and circular polarization at a fixed trap depth of 50 μm from the inner wall of the cover glass. The trap stiffness per beam power for each degree of freedom is found by the linear fit of the experimental data: $(k'_x, k'_y, k'_z) = (1.21, 1.74, 0.27)$ pN/ $\mu\text{m}/\text{mW}$ for a linearly polarized trapping beam and $(k'_x, k'_y, k'_z) = (1.47, 1.48, 0.27)$ pN/ $\mu\text{m}/\text{mW}$ for a circularly polarized trapping beam.

4. Concluding remarks

We demonstrated a method of controlling the stiffness asymmetry of an optical trap (i.e., k_x and k_y) in a highly focused OT setup using the polarization state of trap beam as a control knob. A 300 nm polystyrene sphere was used as a local probe for monitoring the polarization-dependent optical potential. For a linearly polarized trapping beam, the stiffness asymmetry factor s_A was estimated to be 0.29 from the experiment and 0.28 from the GLMT calculation showing reasonable agreement. For the balanced potential formed by a circularly polarized trapping beam, the angular measurements of the

stiffnesses $k_x(\theta)$ and $k_y(\theta)$ show less than 1.5% variation, yielding an s_A value of ~ 0.03 which is one order of magnitude lower than the stiffness asymmetry factor associated with the linear polarization. Our research implies that the polarization state of trap laser beam could be used as a control parameter for adjusting potential landscape in optical tweezers' experiments, which could be of interest in the relevant research fields, e.g., studying the interaction dynamics of colloidal systems in the context of highly focused optical potential.

ACKNOWLEDGEMENT

This work was supported by the research fund of Chonbuk National University in 2015 and by the Basic Science Research Program through the National Research Foundation of Korea (NRF) funded by the Ministry of Education, Science, and Technology (No. 2011-0014908).

REFERENCES

1. A. Ashkin, "Acceleration and Trapping of Particles by Radiation Pressure," *Phys. Rev. Lett.* **24**, 156-159 (1970).
2. A. Ashkin, J. M. Dziedzic, J. E. Bjorkholm, and S. Chu, "Observation of a Single-Beam Gradient Force Optical Trap for Dielectric Particles," *Opt. Lett.* **11**, 288-290 (1986).
3. D. E. Chang, C. A. Regal, S. B. Papp, D. J. Wilson, J. Ye, O. Painter, H. J. Kimble, and P. Zoller, "Cavity opto-mechanics using an optically levitated nanosphere," *Proc. Natl. Acad. Sci. U.S.A.* **107**, 1005-1010 (2010).
4. B. Tränkle, M. Speidel, and A. Rohrbach, "Interaction dynamics of two colloids in a single optical potential," *Phys. Rev. E* **86**, 021401 (2012).
5. M. N. Romodina, M. D. Khokhlova, E. V. Lyubin, and A. A. Fedyanin, "Direct measurements of magnetic interaction-induced cross-correlations of two microparticles in Brownian motion," *Sci. Rep.* **5**, 10491 (2015).
6. M. G. Donato, J. Hernandez, A. Mazzulla, C. Provenzano, R. Saija, R. Sayed, S. Vasi, A. Magazzu, P. Pagliusi, R. Bartolino, P. G. Gucciardi, O. M. Marago, and G. Cipparrone, "Polarization-dependent optomechanics mediated by chiral microresonators," *Nat. commun.* **5**, 3656 (2014).
7. Y. Arita, M. Mazilu, and K. Dholakia, "Laser-induced rotation and cooling of a trapped microgyroscope in vacuum," *Nat. commun.* **4**, 2374 (2013).
8. F. Gittes, and C. F. Schmidt, "Interference model for back-focal-plane displacement detection in optical tweezers," *Opt. Lett.* **23**, 7-9 (1998).
9. D. G. Grier, "A revolution in optical manipulation," *Nature* **424**, 810-816 (2003).
10. A. Rohrbach, "Stiffness of Optical Traps: Quantitative Agreement between Experiment and Electromagnetic Theory," *Phys. Rev. Lett.* **95**, 168102 (2005).
11. A. R. Zakharian, P. Polynkin, M. Mansuripur, and J. V. Moloney, "Single-beam trapping of microbeads in polarized light: Numerical simulations," *Opt. Express* **14**, 3660-3676 (2006).

12. E. Madadi, A. Samadi, M. Cheraghian, and S. N. S. Reihani, "Polarization-induced stiffness asymmetry of optical tweezers," *Opt. Lett.* **37**, 3519-3521 (2012).
13. M. Mansuripur, "Distribution of Light at and near the Focus of High-Numerical-Aperture Objectives," *J. Opt. Soc. Am. A* **3**, 2086-2093 (1986).
14. P. Török, P. Varga, Z. Laczik, and G. R. Booker, "Electromagnetic Diffraction of Light Focused through a Planar Interface between Materials of Mismatched Refractive-Indexes - an Integral-Representation," *J. Opt. Soc. Am. A* **12**, 325-332 (1995).
15. A. Mahmoudi, and S. N. S. Reihani, "The effect of immersion oil in optical tweezers," *Opt. Express* **19**, 14794-14800 (2011).
16. J. P. Barton, and D. R. Alexander, "Fifth-order corrected electromagnetic field components for a fundamental Gaussian beam," *J. Appl. Phys.* **66**, 2800 (1989).
17. J. P. Barton, D. R. Alexander, and S. A. Schaub, "Theoretical determination of net radiation force and torque for a spherical particle illuminated by a focused laser beam," *J. Appl. Phys.* **66**, 4594 (1989).
18. W. M. Lee, P. J. Reece, R. F. Marchington, N. K. Metzger, and K. Dholakia, "Construction and calibration of an optical trap on a fluorescence optical microscope," *Nat. Protoc.* **2**, 3226-3238 (2007).
19. L. Friedrich, and A. Rohrbach, "Tuning the detection sensitivity: a model for axial backfocal plane interferometric tracking," *Opt. Lett.* **37**, 2109-2111 (2012).
20. S. N. S. Reihani, S. A. Mir, A. C. Richardson, and L. B. Oddershede, "Significant improvement of optical traps by tuning standard water immersion objectives," *J. Opt.-UK* **13**, 105301 (2011).
21. K. Berg-Sørensen, and H. Flyvbjerg, "Power spectrum analysis for optical tweezers," *Rev. Sci. Instrum.* **75**, 594 (2004).
22. P. M. Hansen, I. M. Tolic-Nørrelykke, H. Flyvbjerg, and K. Berg-Sørensen, "tweezercalib 2.1: Faster version of MatLab package for precise calibration of optical tweezers," *Comput. Phys. Commun.* **175**, 572-573 (2006).

Figure Captions.

Fig. 1. (a) Schematic diagram of the experimental setup with a Cartesian coordinate system (x, y, z). HWP: half wave plate. PBS: polarizing beam splitter. QWP: quarter wave plate. Obj. L: a water-immersion objective lens with correction collar. L1 and L2: condenser lens and relay lens, respectively. QPD: quadrant photodiode. LED: light-emitting diode. The dichroic mirror (DM) is removed during power spectral density (PSD) measurements. (b) Part of QPD outputs: δv_x (red) and δv_y (blue). (c) PSD of QPD outputs: empty circles (red) and empty squares (blue) represent the PSD of δv_x and δv_y , respectively. Black and gray lines represent the PSD of system noise without any trapped particles. The two vertical lines indicate the corner frequencies: $f_{c,x}$ (red solid line) and $f_{c,y}$ (blue dotted line).

Fig. 2. (a) The normalized electric field strength distribution for a linearly polarized input trapping beam at the focal plane. (b) Upper panel: solid and dashed curves represent intensity profiles along the lines L_x and L_y , respectively. Lower panel: solid (δI_{L_x}) and dashed (δI_{L_y}) curves represent the difference between the fifth-order Gaussian beam method and the method based on vectorial diffraction theory. (c) Generalized Lorenz-Mie theory (GLMT) force calculation for a 300 nm polystyrene particle trapped in the linearly polarized beam. Solid and dashed curves represent optical forces F_x and F_y along L_x and L_y , respectively.

Fig. 3. (a) The normalized electric field strength distribution for a circularly polarized input trapping beam at the focal plane. (b) Upper panel: red and blue dashed curves represent intensity profiles along the lines L_x and L_y , respectively. Lower panel: red (δI_{L_x}) and blue (δI_{L_y}) dashed curves represent the difference between the fifth-order Gaussian beam method and the method based on vectorial diffraction theory. (c) Generalized Lorenz-Mie theory (GLMT) force calculation for a 300 nm polystyrene particle trapped in the circularly polarized beam: Red and blue dashed curves represent optical forces along L_x and L_y , respectively.

Fig. 4. The red, solid curves and the blue, dashed curves represent theoretical calculations of trap stiffnesses k_x and k_y , respectively. (a) Angle (θ_{HWP}) dependence of k_x (\bullet) and k_y (\blacksquare). (b) Trap stiffnesses k_x (\bullet) and k_y (\blacksquare) as a function of the polarization state presented in terms of the QWP angle (θ_{QWP}).

Fig. 5. (a) Trap stiffnesses variation $k_x(\theta)$ (\bullet) and $k_y(\theta)$ (\blacksquare) of the balanced potential. (b) Trap stiffness as a function of trap beam power. The square, circular, and triangular symbols denote k_x , k_y , and k_z , respectively, and the filled and empty symbols denoted the linear and circular polarization states, respectively. For most data points, the error bars ($\pm 1\sigma$ level) are smaller than the size of the symbols.

Figures

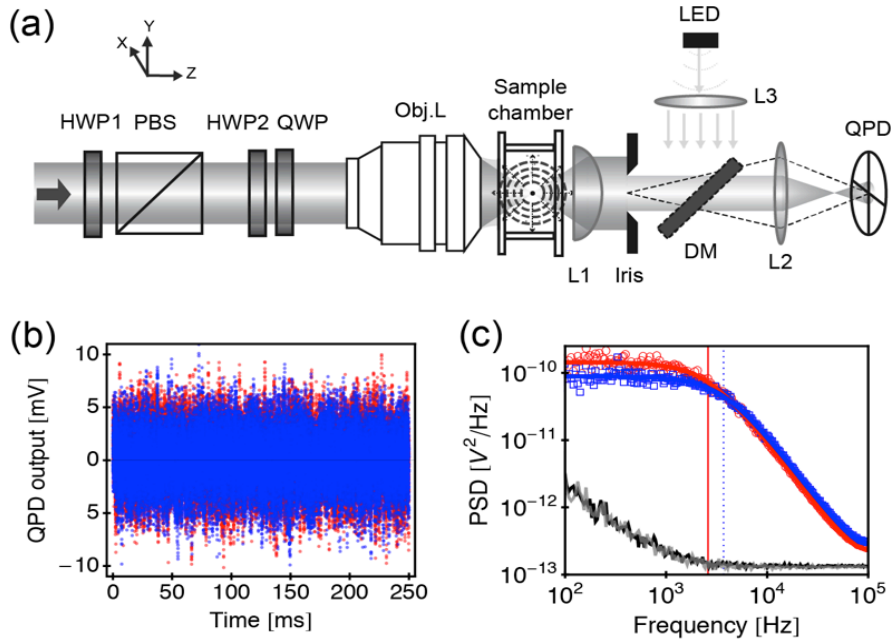


Fig. 1

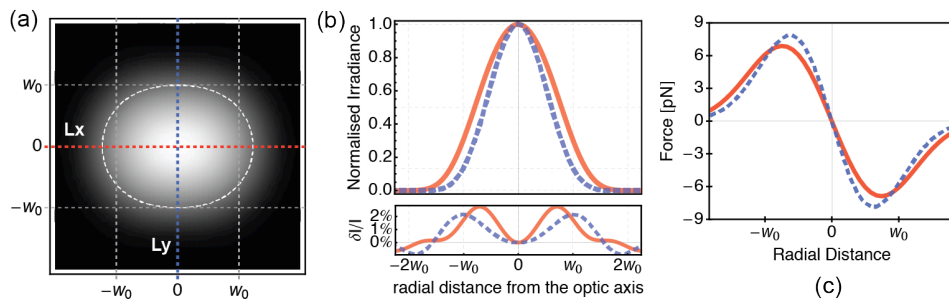


Fig. 2

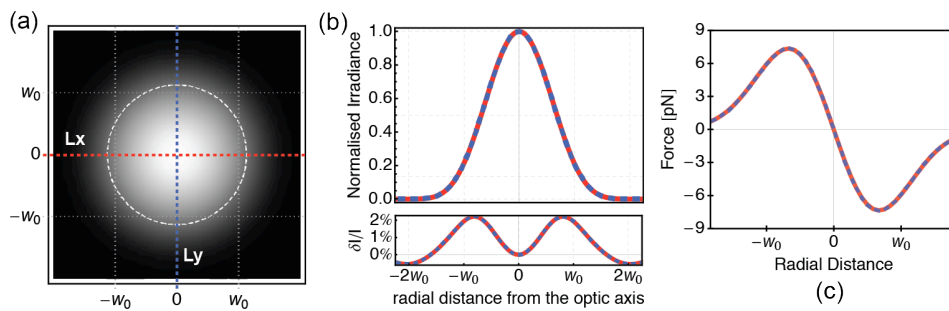


Fig. 3

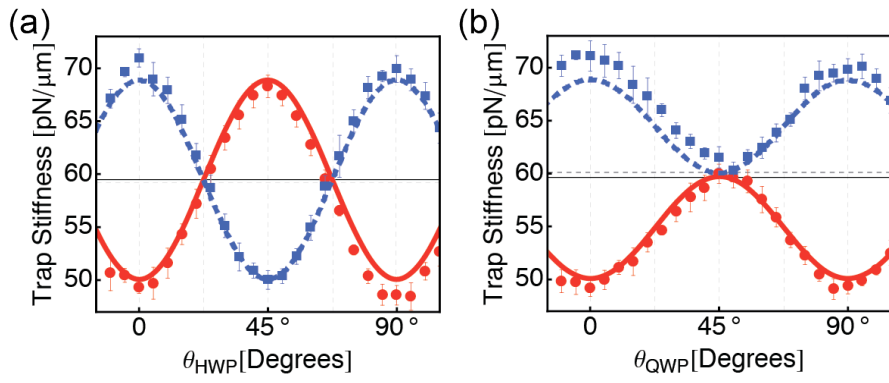


Fig. 4

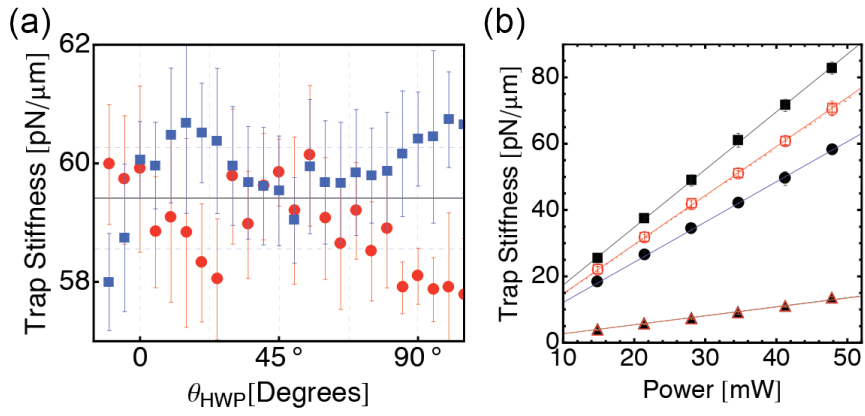


Fig. 5